Recognition and Activation of the Plant AKT1 Potassium Channel by the Kinase CIPK23[1[OPEN]]

María José Sánchez-Barrena,[a] Antonio Chaves-Sanjuan,[a] Natalia Raddatz,[b] Imelda Mendoza,[b] Álvaro Cortés,[c] Federico Gago,[c] Juana María González-Rubio,[a] Juan Luis Benavente,[a] Francisco J. Quintero,[b] José M. Pardo,[b,2] and Armando Albert[a,2,3]

[a]Departamento de Cristalografía y Biología Estructural, Instituto de Química Física "Rocasolano", Consejo Superior de Investigaciones Científicas, E-28006 Madrid, Spain
[b]Instituto de Bioquímica Vegetal y Fotosíntesis, Consejo Superior de Investigaciones Científicas-Universidad de Sevilla, E-41092 Sevilla, Spain
[c]Área de Farmacología, Departamento de Ciencias Biomédicas, Unidad Asociada al Instituto de Química Médica-Consejo Superior de Investigaciones Científicas, Universidad de Alcalá, E-28006 Madrid, Spain

ORCID IDs: 0000-0002-5986-1804 (M.J.S.-B.); 0000-0003-3287-9024 (A.C.-S.); 0000-0002-2673-3961 (I.M.); 0000-0002-3071-4878 (F.G.); 0000-0001-8718-2975 (F.J.Q.); 0000-0003-4510-8624 (J.M.P.); 0000-0002-0026-6816 (A.A.).

Plant growth largely depends on the maintenance of adequate intracellular levels of potassium (K^+). The families of 10 Calcineurin B-Like (CBL) calcium sensors and 26 CBL-Interacting Protein Kinases (CIPKs) of Arabidopsis (*Arabidopsis thaliana*) decode the calcium signals elicited by environmental inputs to regulate different ion channels and transporters involved in the control of K^+ fluxes by phosphorylation-dependent and -independent events. However, the detailed molecular mechanisms governing target specificity require investigation. Here, we show that the physical interaction between CIPK23 and the noncanonical ankyrin domain in the cytosolic side of the inward-rectifier K^+ channel AKT1 regulates kinase docking and channel activation. Point mutations on this domain specifically alter binding to CIPK23, enhancing or impairing the ability of CIPK23 to regulate channel activity. Our data demonstrate the relevance of this protein–protein interaction that contributes to the formation of a complex between CIPK23/CBL1 and AKT1 in the membrane for the proper regulation of K^+ transport.

Potassium (K^+) serves important roles in plants for the control of cellular pH, regulation of membrane electric potentials and cell turgor, and as a cofactor in essential metabolic processes including protein synthesis (Leigh and Wyn Jones, 1984; Rodríguez-Navarro, 2000; Pardo, 2010; Chérel and Gaillard, 2019; Ragel et al., 2019). Several ion transporters mediating K^+ fluxes in plants have been characterized, and the knowledge of their activity in response to environmental stresses and the molecular mechanisms underlying their regulation has been central for understanding the adaptation to K^+ starvation (Chérel et al., 2014; Ragel et al., 2015; Lefoulon et al., 2016; Behera et al., 2017), high salinity (Alemán et al., 2014), drought (Maierhofer et al., 2014), and to pathogen attack or herbivore-mediated wounding (Forster et al., 2019)

The family of plasma membrane voltage-gated (VG) K^+ channels is crucial for K^+ uptake, release, and distribution at the cellular and whole plant levels. In Arabidopsis (*Arabidopsis thaliana*), this channel family comprises nine members that display different roles in K^+ nutrition and cellular physiology (Pilot et al., 2003). For instance, the Guard cell Outward-Rectifying K^+ (GORK) channel is crucial for mediating K^+ efflux from guard cells, thereby reducing cell turgor and inducing stomatal closure (Ache et al., 2000; Hosy et al., 2003; Hedrich and Geiger, 2017), whereas the inward-rectifier K^+ channel AKT1 is highly expressed in root epidermal cells and is a major contributor to K^+ uptake at intermediate to high K^+ concentrations (Lagarde et al., 1996; Hirsch et al., 1998; Xu et al., 2006; Wang et al., 2010; Alemán et al., 2011; Jegla et al., 2018). Functional GORK1 and AKT1 are tetramers whose subunits display an N-terminal transmembrane domain that is homologous to the animal VG *Shaker* channels, and a large cytoplasmic domain that consists of a cyclic nucleotide-binding homologous domain (CNBHD), followed by

[1]This work was funded by Agencia Estatal de Investigación (AEI, Spain) and Fondo Europeo de Desarrollo Regional (FEDER, European Union) (BIO2017-89523-R to A.A., BIO2015-70946-R to F.J.Q., BIO2016-81957-REDT to J.M.P., and RTI2018-094027-B-I00 to J.M.P.)
[2]Senior authors.
[3]Author for contact: xalbert@iqfr.csic.es.
The author responsible for distribution of materials integral to the findings presented in this article in accordance with the policy described in the Instructions for Authors (www.plantphysiol.org) is: Armando Albert (xalbert@iqfr.csic.es).
A.C.-S., M.J.S.-B., J.M.G.-R., J.L.B., A.C., N.R., and I.M. performed experiments; F.G., F.J.Q., J.M.P., and A.A. designed and supervised the project; M.J.S.-B., F.J.Q., J.M.P., and A.A. participated in the experimental design and wrote the article.
[OPEN]Articles can be viewed without a subscription.
www.plantphysiol.org/cgi/doi/10.1104/pp.19.01084

an ankyrin (ANK) repeat domain and a characteristic family-conserved (KHA, plant K^+ channel motif rich in hydrophobic and acidic residues) motif at the C-terminal end (Daram et al., 1997; Pilot et al., 2003; Jegla et al., 2018). While the transmembrane domain harbors the ion transport activity, the cytosolic moiety is involved in channel regulation. Available data suggest a common regulatory mechanism for GORK and AKT1 in which a protein complex between a Calcineurin B-like (CBL) and a CBL-Interacting Protein Kinase (CIPK; Shi et al., 1999; Albrecht et al., 2001) decodes a specific calcium signature to phosphorylate and activate K^+ transport. While the CIPK5/CBL1 pair is responsible for GORK1 activation in response to wounding (Forster et al., 2019), CIPK23/CBL1 or CIPK23/CBL9 pairs activate AKT1 upon a signal elicited by K^+ starvation (Xu et al., 2006). Depending on the K^+ status, the protein phosphatases AIP1 and ABI2 would revert this process and dephosphorylate AKT1 and GORK1, respectively (Lee et al., 2007; Lan et al., 2011; Lefoulon et al., 2016).

To achieve the necessary specificity of protein–protein interactions, the CIPK/CBL modules and their targets have coevolved discrete scaffold domains or small sequence motifs that mediate and control the interactions (Lan et al., 2011; Sánchez-Barrena et al., 2013). For instance, the interaction between CIPKs and CBLs occurs through a conserved 21 amino acid NAF motif, which is self-inhibitory to the kinase activity (Albrecht et al., 2001; Guo et al., 2001; Sánchez-Barrena et al., 2007). CBL binding releases the NAF domain from the substrate binding site of CIPKs, making it accessible to phosphorylate their substrate channels (Chaves-Sanjuan et al., 2014b). CIPKs also harbor a Protein Phosphatase Interaction motif that constitutes a structural domain mediating the interaction with PP2C protein phosphatases (Gong et al., 2004; Sánchez-Barrena et al., 2007; Luan, 2009). Full activation of K^+ transport by AKT1 requires the physical interaction with the CIPK23/CBL1-9 module (Xu et al., 2006), and phosphorylation of CBL1 by CIPK23 further stabilizes the complex (Hashimoto et al., 2012). Moreover, CBL1 and CBL9 have a myristoylation site in the N-terminus that recruits these complexes to the cell membrane in the vicinity of AKT1 (Batistic et al., 2010). In addition, the physical interaction between the CIPK23/CBL1-9 complex and AKT1 is required to achieve the necessary target specificity and regulation of the system (Xu et al., 2006). We have reported structural and biochemical studies demonstrating that CIPK23 is intrinsically inactive (Chaves-Sanjuan et al., 2014b). Presumably, the colocalization of the kinase and its substrate channel may favor kinase activation, with the subsequent phosphorylation and activation of the channel. Together, these data indicate that AKT1, and likely GORK also, are held together with their regulatory proteins into a large macromolecular complex with variable composition and stoichiometry, which is necessary to achieve specificity of the signal and to develop the physiological role of these channels.

The interaction between CIPK23 and AKT1 is known to involve the ankyrin domain of AKT1 and the kinase domain of CIPK23, and it has been suggested that this interaction could be a factor to determine which specific CIPKs attach to the AKT1 channel (Lee et al., 2007). ANK motifs are well known protein–protein interaction modules that usually play a passive regulatory role in the formation of protein complexes (Sedgwick and Smerdon, 1999). However, the discovery of phosphomimetic mutations in or at the vicinity of the ANK domain of GORK that increase the activity of the channel (Lefoulon et al., 2016) suggests that the ANK domain of plant VG channels may display a regulatory role in the activity of the channel. To gain insights into the function of the ANK domain of AKT1, and more specifically on the regulation of AKT1 by CIPKs, we carried out biochemical and structural studies, including solving the x-ray structure of the ANK domain of AKT1 and measuring the channel activity resulting from structure-guided mutations altering the ANK domain. Our results show that the ANK domain of AKT1 functions as a platform for docking of the catalytic domain of CIPK23, and that this interaction contributes to the activation of the channel by promoting the formation of a productive CIPK-AKT1 complex.

RESULTS

The Structure of the ANK Domain of AKT1

The ankyrin domain typically comprises several tandemly repeated ANK motifs consisting of two α-helices separated by loops that together form a slightly curved solenoid structure. To define the molecular architecture and the surface properties of the ANK domain of AKT1, we determined the x-ray structure of the AKT1 fragment comprising residues 516–706 at 2.0 Å resolution (see "Materials and Methods" for further details; Fig. 1; Supplemental Table S1). The ANK domain fragment folds as a single domain formed by six ANK-unit repeats. Of them, the ANK repeats 1, 2, 4, and 5 are canonical and display the characteristic α-helix/α-helix/β-hairpin structure while the ANK repeats 3 and 6 lack the β-hairpin. This feature is common to other known C-terminal capping ANK repeats (Mosavi et al., 2002), but was not expected from the amino acid sequence analysis of ANK repeat 3 (Daram et al., 1997). Those amino acids predicted to form the β-hairpin of ANK repeat 3 constitute an extra turn at the N-terminal helix of the ANK repeat 4. This arrangement renders an elongated and curved structure formed by two layers of six antiparallel α-helices and a sheet formed by four (instead of five) β-hairpins projected perpendicularly from the concave side. The association of canonical ANK repeats produce a characteristic and conserved domain curvature that leaves the concave side available for binding partners (Michaely et al., 2002). In the ANK domain of AKT1, this structure is distorted and a more concave surface is

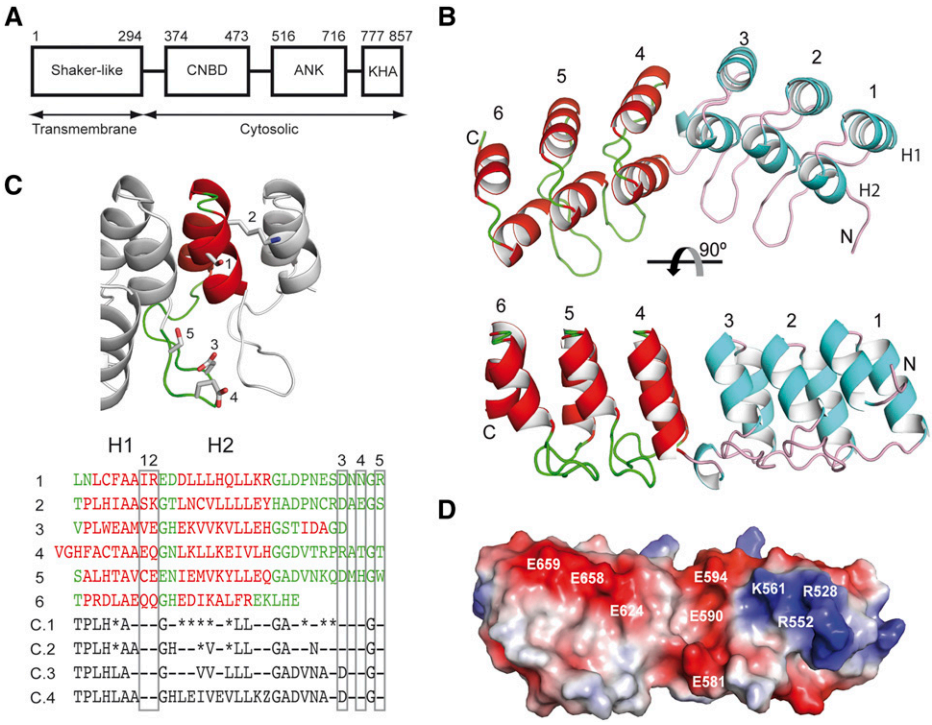

Figure 1. Structure of the ANK domain of AKT1. A, Functional and structural domains of AKT1. B, Two views of a ribbon representation of the crystal structure of the ANK domain. The ANK repeats are numbered. H1 and H2 helices stand for those helices facing inwards or outwards of the concave side of the structure, respectively. C, Upper, a detailed view of the structure of the ANK repeat 2. The variable side chains are highlighted in stick mode. Lower, sequence alignment of the six ANK repeats of AKT1 together with the ANK consensus sequences according to different authors: C.1 (Mosavi et al., 2002), C.2 (Michaely et al., 2002), C.3 (Sedgwick and Smerdon, 1999), and C.4 (Kohl et al., 2003). Red and green colors stand for helical and loop regions, respectively. D, Molecular surface representation showing the charge distribution on the ANK domain. The red and blue colors correspond to negative and positive charges, respectively. The view is taken as in the lower part of (B).

observed due to the lack of the β-hairpin at ANK repeat 3 (Supplemental Fig. S1).

With the exception of the mentioned singularities, all the repeats show similarity with the ANK-repeat consensus sequence. This conservation includes mainly those residues involved in the boundaries of the secondary structural elements, in the core of the individual repeats and in the repeat-repeat stabilization (Fig. 1C; Michaely et al., 2002; Mosavi et al., 2002). On the contrary, those residues known to be variable in ANK repeats are solvent-accessible, with those facing inwards toward the concave side of the domain being involved in the interaction with the binding partners (Fig. 1C, residues at positions 1–5; Sedgwick and Smerdon, 1999; Mosavi et al., 2002). These amino acids define the nature of the protein–protein interaction surface and are therefore responsible for the specificity of the interaction (Tamaskovic et al., 2012). Interestingly, the basic residues Arg-528 and Lys-561 at position 1 of ANK repeats 1 and 2 oppose the acidic residues Glu-594 and Glu-659 at the equivalent position of ANK repeats 3 and 5. This amino acid distribution yields a highly asymmetric charge distribution in the surface of the ANK domain that is reinforced by Arg-552 versus Asp-581, Glu-624, and Glu-690, in stark contrast with the symmetric architecture of the tertiary structure of the domain (Fig. 1D).

We reasoned that these structural peculiarities could provide the basis for the ANK function in the protein-interaction specificity of AKT1. To analyze this issue, we aligned the protein sequences of the ANK domains of seven Arabidopsis K^+ channels and compared the result to the alignment of protein sequences annotated as AKT1-like channels from other plant species (Supplemental Fig. S2). The comparison showed that the overall architecture of the ANK domain should be preserved in all the channels, as there are no residue insertions or gap regions with the exception of the last ANK repeat of AtAKT2. However, the alignment also shows that while the nature of the key residues configuring the surface properties of the concave side of the AKT1 domain are conserved among different plant species, they diverge between the different Arabidopsis K^+ channels. This suggests that the ANK domain of individual channels is likely to play an active role, providing specificity to the interaction with protein partners involved in their regulation.

The crystal packing of the ANK domain does not reveal any interaction suggestive of self-association (Krissinel and Henrick, 2007). To examine the oligomeric state of the ANK domain in solution, we determined the ANK peptide size in solution by size exclusion chromatography (SEC). Results showed the monomeric nature of the ANK domain (Supplemental Fig. S3A), and suggested that the ANK domain of AKT1 is fully available to interact with CIPK23.

The Properties of the Complex between the ANK Domain of AKT1 and the Catalytic Domain of CIPKs

The structure of the ANK domain of AKT1 provides the basis to investigate the nature of CIPK23-AKT1 association. We performed yeast two-hybrid (Y2H) assays using the full-length CIPK23 protein, the complete cytosolic domain of AKT1 (AKT1cyt; residues

296–857), and two mutated versions changing the polarity of the concave side of the ANK domain, namely AKT1(−) for the Arg-528Glu and Lys-561Glu double mutant, and AKT1(+) for the Glu-624Lys, Glu-658Lys, and Glu-659Lys triple mutant (Fig. 2). The results confirmed that CIPK23 interacts with AKT1cyt (Lee et al., 2007). Interestingly, the replacement of the basic residues at the concave side of the ANK domain with acidic residues in AKT1(−) did not affect the interaction of the AKT1 fragment with the kinase in the Y2H assay, whereas the replacement of the acidic residues with basic residues in AKT1(+) disrupted the interaction. These findings corroborate the involvement of the concave side of the ANK domain in the interaction with CIPK23 and demonstrate the electrostatic nature of the interaction.

To investigate whether the properties of the ANK domain provide specificity for CIPK23 versus other CIPKs, we repeated the Y2H assays using CIPK16 and CIPK24. CIPK16 has been shown to interact with the C-terminal tail of AKT1 and also to activate AKT1 transport in a CBL1-dependent manner, although the induced K^+ current was much lower than the one elicited by CIPK23 coexpression (Lee et al., 2007; Fig. 2). By contrast, CIPK24 did not interact with AKT1 (Lee et al., 2007). Our data confirm these previous results and show that the mutations on the concave side of the ANK domain affecting formation of the AKT1/CIPK23 complex do not significantly alter the interaction with CIPK16, thus proving that the structure of the ANK domain in AKT1 provides specificity to the CIPK23-AKT1 interaction.

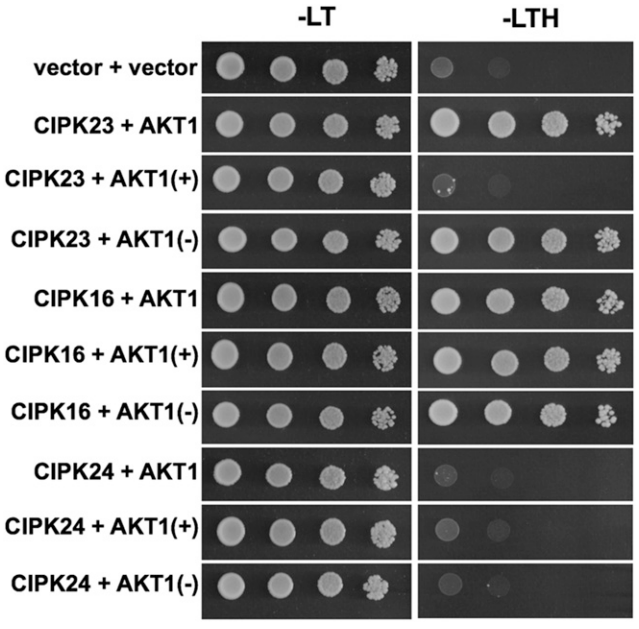

Figure 2. Electrostatic interactions are critical for CIPK23/AKT1 complex stability. Y2H assay of full-length CIPK23, CIPK16, or CIPK24 and the wild-type AKT1 C-terminal domain (residues 296–857) or mutant versions AKT1(+) for Glu-624Lys, Glu-658Lys, and Glu-659Lys; and AKT1(−) for Arg-528Glu and Lys-561Glu. Five microliters of serial decimal dilutions of yeast cultures were spotted onto SD−LT plates or SD−LTH plates. Growth on SD−LTH medium indicates protein–protein interaction.

Next, we determined the dissociation constant (K_d) of the complex between the ANK domain of AKT1 and its mutated versions with the catalytic domain of CIPK23. For the binding assay, the purified and uncleaved versions AKT1(−) and AKT1(+) of the His-tagged ANK domain were immobilized on a nickel-chelated biosensor tip, and the binding of the constitutively activated form of the CIPK23 catalytic domain (residues 1–331, CIPK23HA, harboring phosphomimetic mutation Thr-190Asp in the activation loop; Chaves-Sanjuan et al., 2014b) was recorded by biolayer interferometry. In this technique, as CIPK23HA binds to the immobilized ANK domain, incident light directed through the biosensor shifts and creates a quantifiable interference pattern. A quantitative equilibrium constant, K_d, can be measured by analyzing this response at different ligand concentrations (Sultana and Lee, 2015). Our data show that the K_d values of the wild-type ANK domain and AKT1(−) with CIPK23HA are 0.98 ± 0.05 μM and 0.68 ± 0.05 μ M, respectively (Supplemental Fig. S3B). These values are consistent with those reported for other physiologically relevant but weak non-obligate protein–protein interactions involved in signal transduction processes (Nooren and Thornton, 2003; Keskin et al., 2008; Perkins et al., 2010). These results signify that mutations leading to AKT1(−) fragment improve the interaction with CIPK23. Conversely, as observed in the Y2H assays, we were not able to detect AKT1(+) binding to CIPK23HA by biolayer interferometry (Supplemental Fig. S3B).

Strengthening the Interaction between CIPK23 and the ANK Domain of AKT1 Contributes to Channel Activation

Previous studies have shown that the physical interaction between AKT1 and CIPK23 is absolutely required for channel activation (Xu et al., 2006; Lee et al., 2007), and that the ANK domain of AKT1 is central for this interaction (Lee et al., 2007). To investigate whether the ANK domain mediates the recruitment of CIPK23 before channel phosphorylation and activation, we coexpressed full-length AKT1 channels harboring the mutated AKT1(−) and AKT(+) domains, together with the catalytically activated version of CIPK23, CIPK23HA, in *Xenopus laevis* oocytes and measured AKT1 activity (Fig. 3). CIPK23HA was able to activate wild-type AKT1 to the same level as shown in Lee et al. (2007). Notably, the AKT1(−) variant increased channel activity above that of the wild-type AKT1, whereas the AKT1(+) mutation almost abolished it. These results are consistent with the Y2H data and the calculated K_d values for the ANK domain and CIPK23 interaction and demonstrate that (1) the interaction of CIPK23 with the ANK domain of AKT1 not only facilitates but is essential for the CIPK23-mediated

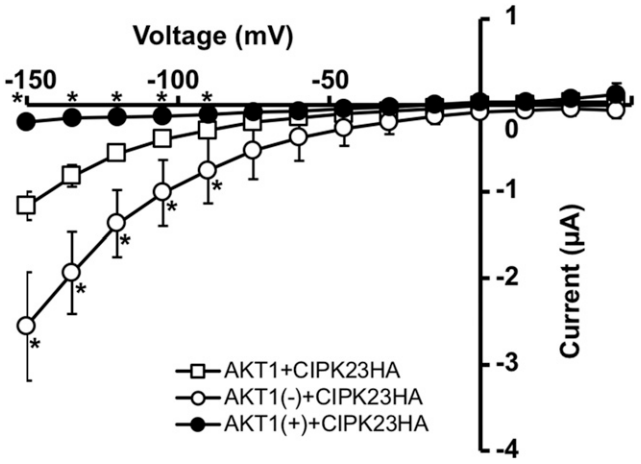

Figure 3. The strength of the binding of the catalytic domain of activated CIPK23 (CIPK23HA) to the ANK domain of AKT1 influences channel activity. Current–voltage relationships recorded from oocytes expressing wild-type AKT1 + CIPK23HA (n = 5), AKT1(+) + CIPK23HA (n = 4), and AKT1(−) + CIPK23HA (n = 4). The bath solution contained 100 mM of KCl. Holding potential was −20 mV. Clamp potentials ranged from +45 to −150 mV with 15-mV decrements during 150 ms, separated by intervals of 2 s. Average currents from water-injected oocytes at each voltage have been subtracted. Data are shown as mean ± SD. The number of oocytes per experiment is indicated in parentheses. Asterisks indicate significant differences compared to wild-type AKT1 + CIPK23HA (Student's t test, $P < 0.05$).

activation of the channel, and that (2) the strength of this interaction is related with channel activation in vivo.

The ANK Domain of AKT1 Is Not Essential for K^+ Transport

The presence of ANK domains is a feature common to several tetrameric cation channels with known structure, among them the nonselective cation channels TRPA1 (Paulsen et al., 2015) and TRPV1 (Gao et al., 2016), the VG potassium (K_v) channels, and the lipid-gated cation channel TRPC3 (Tang et al., 2018). Despite this structural commonality, the role of the ANK domains in the function and/or the regulation of these channels remains to be elucidated. Their high-resolution structures showed that these ANK domains are likely essential for channel activity because they display intermolecular interactions between them and with other domains of different protomers making up the channels, thus contributing to macromolecule stabilization, and/or being involved in the transduction of information from the cytosolic domain to the transmembrane pore. On the contrary, previously reported Y2H analysis showed that while the cytosolic domain of AKT1 is self-assembled into tetramers, the ANK domain does not interact with the other domains comprising the protein structure of AKT1 (Daram et al., 1997). To determine whether the ANK domain of AKT1 is required for K^+ transport, we tested the functionality of full-length AKT1 in a yeast mutant defective in K^+ uptake and compared it to that of a mutated AKT1 protein lacking the ANK domain. This assay has the advantage that the basal AKT1 transport activity in the absence of CIPK23 is robust enough to support yeast growth at low external K^+ concentrations, likely due to large negative membrane potentials in K^+-starved yeast cells. Our results showed that the AKT1 channel lacking the ANK domain was functionally expressed in yeast and restored cell growth at low K^+ concentrations similarly to the wild-type channel (Fig. 4). Next, we tested the functionality of the mutated forms of the channel leading to AKT1(−) and AKT1(+). Both mutated channels behaved as the wild-type channel, indicating that the mutated proteins were expressed and that the change in the polarity of the ANK domain did not affect the transport mechanism of the channel (Fig. 4). Together, these results show that the ANK domain is not essential for AKT1 function or stability and suggests that it would be mostly involved in the recruitment of regulatory proteins, e.g. CIPK23, to the vicinity of the channel.

The Structure of the Complex between the ANK Domain of AKT1 and the Catalytic Domain of CIPK23

Attempts to crystallize the protein complex between the ANK domain of AKT1 and the CIPK23 kinase were unsuccessful. Instead, we took advantage of the structural knowledge of the ANK domain of AKT1 and of the catalytic domain of CIPK23 (Chaves-Sanjuan et al., 2014b) to define an integrative three-dimensional working model of this complex. Previous Y2H data

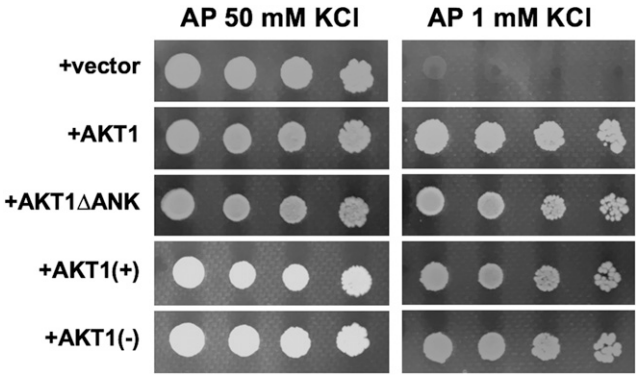

Figure 4. The ANK domain of AKT1 is not required for K^+ transport and mutations in AKT1(+) or AKT1(−) do not affect channel transport activity. Cells of yeast strain 9.3 (Δ*trk1*, Δ*trk2*) were transformed with the empty vector pFL61 (+vector), the wild-type *AKT1* cDNA (+AKT1), the mutant *AKT1* allele lacking the ankyrin repeat coding region (+AKT1ΔANK), or the mutated versions of *AKT1*: +AKT1(+) and +AKT1(−). Transformed yeast cells were grown overnight in AP medium with 50 mM of KCl. Five microliters of serial decimal dilutions were spotted onto AP plates supplemented with the indicated KCl concentration.

(Lee et al., 2007) showed that the helical lobe of the kinase domain was responsible for the interaction with the ANK domain, and we have shown earlier that residues at both ends of this lobe cluster together on the structure of CIPK23 (Fig. 5A; Supplemental Fig. S4; Chaves-Sanjuan et al., 2014b). This experimental information substantially improved the performance of the computational work, as it provided an experimental criterion to define the resulting structure.

To build de novo the three-dimensional structure of the CIPK23-ANK domain complex, we first generated a set of models based on the crystal structure of CIPK23 and of the ANK domain that accounted for the predicted conformational variability of the proteins. Then, we selected those docking solutions that correctly involved the experimentally determined residues as participants in the interaction. Finally, we performed molecular dynamics (MD) simulations on the best solution to optimize the geometry of the amino acid side chains involved in the interaction. The modeled CIPK23-ANK complex displays a rocking chair shape in which the kinase active site and the regulatory activation-loop of CIPK23 remain unaltered and solvent-accessible upon complex formation. This indicates that the CIPK23 function would be unaffected upon complex formation and that a regulatory role for the ANK domain on the kinase activity is not expected.

The modeled structure indicates that CIPK23 and the ANK domain interact through the concave side of the ANK domain. The total buried accessible area per protomer is 1,050 A^2, and 90% of this occluded area corresponds to polar residues (Hubbard and Thornton, 1993). These values are similar to those expected for non-obligate oligomers in solution (Nooren and Thornton, 2003; Krissinel and Henrick, 2007; Perkins et al., 2010).

According to this model, Glu-624 and Glu-658 are totally buried in the CIPK23/ANK interface making polar contacts with CIPK23 (Fig. 5B). This agrees with our biochemical data showing that mutation of both residues to Lys in AKT1(+) abolishes the CIPK23/ANK interaction and subsequent activation of AKT1. Conversely, the effect of mutations Arg-528Glu and Lys-561Glu leading to the AKT1(−) variant is more difficult to rationalize in terms of our model, because Arg-528 is not involved in the interaction with CIPK23, while Lys-561 is hydrogen-bonded to the kinase (Fig. 5C).

DISCUSSION

The automatic analysis of the AKT1 protein sequence (Kelley et al., 2015) suggests that the overall structure of the channel is similar to those of the VG K^+ Eag1 channel (Whicher and MacKinnon, 2016) and the HCN1 hyperpolarization-activated channel (Lee and MacKinnon, 2017). These structures display a homotetrameric arrangement of six transmembrane segments divided into the voltage-sensing module and the pore-forming module. The last transmembrane helix connects to a CNBD domain through a helical region that couples motions of the CNBD with those of the channel machinery. Both the helical region and the CNBD display a tetrameric quaternary structure forming two consecutive layers below the transmembrane moiety (Fig. 6). Although there are no high-resolution structures of homologous channels with a C-terminal end containing ANK and KHA domains, it has been shown that the KHA domain is involved in the maintenance of the tetrameric structure of the cytosolic part of the channel through interactions with the CNBHD from a neighboring subunit, while the ANK domain neither interacts with other domains of the channel nor self-associates (Daram et al., 1997; Supplemental Fig. S3). Indeed, we have shown that deletion of the ANK

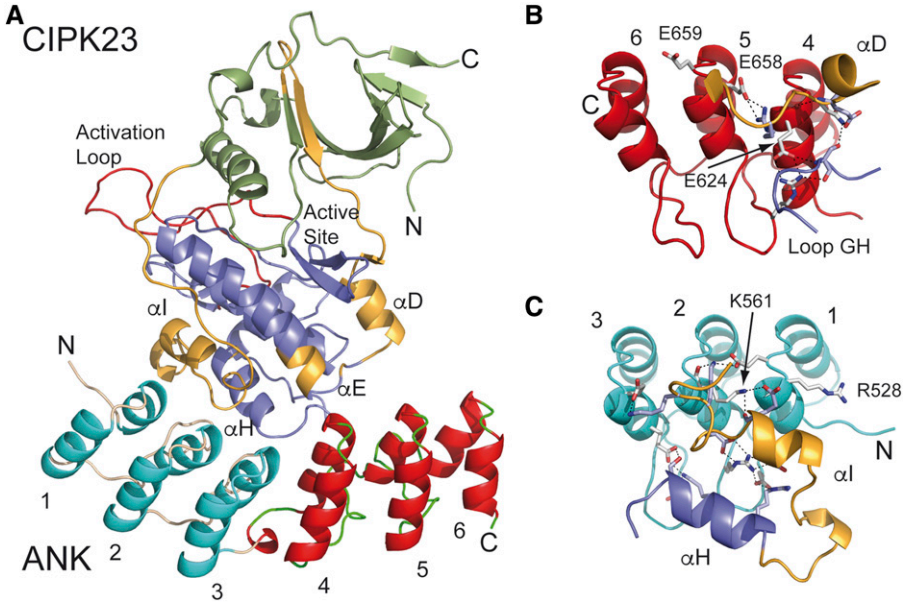

Figure 5. The structure of the complex between the ANK domain of AKT1 and CIPK23. A, A ribbon representation of the predicted model for the CIPK23 and ANK domain of AKT1. Those residues of CIPK23 experimentally determined to be essential for the interaction with AKT1 are displayed in gold color (Lee et al., 2009). B and C, Ribbon representations of the CIPK23 binding site on the ANK domain. Residues involved in the interaction are displayed in stick mode. Those residues leading to the AKT1(+) and AKT1(−) are labeled.

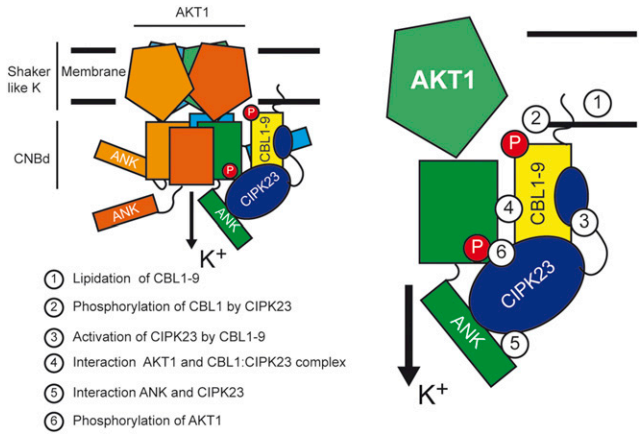

Figure 6. Working model for AKT1 regulation. The effective regulation of AKT1 is achieved when all interaction partners meet nearby AKT1. The reported structural requirements to activate K^+ transport are listed from 1 to 6 in Figure 1. (1) Lipidation of CBL1/CBL9 (Batistic et al., 2010); (2) phosphorylation of CBL1 by CIPK23 (Hashimoto et al., 2012); (3) activation of CIPK23 by CBL1/CBL9 (Albrecht et al., 2001); (4) interaction between AKT1 and CIPK23/CBL1-9 complex (Xu et al., 2006; Lee et al., 2007); (5) interaction of ANK and CIPK23 (Lee et al., 2007) and this work; and (6) phosphorylation of AKT1 (Xu et al., 2006; Hashimoto et al., 2012).

domain did not suppress channel activity in vivo (Fig. 4). Together, these data indicate that the ANK domain would be fully available to interact with CIPK23 and that this interaction would not affect the tetrameric globular structure made up by the transmembrane domain, the CNBHD, and the KHA domains. This provides a model in which the ANK domain functions as a structural platform for the transitory docking of the CIPK23 kinase domain to the vicinity of the channel. According to earlier biochemical evidence (Lee et al., 2007) and our structural data (Fig. 5A), this association would not hinder the catalytic activity of CIPK23, but rather could enhance it. We have shown before that the kinase is constitutively inactive (Chaves-Sanjuan et al., 2014b) or displays weak activity in comparison with other kinases of the family (Hashimoto et al., 2012). Reconstitution of the AKT1-CIPK23 module in *X. laevis* oocytes showed that the strength of the physical interaction between the ANK domain of AKT1 and CIPK23 ultimately determined the ability of the kinase to activate the channel (Fig. 3). Hence, we suggest that the physical interaction with the ANK domain and the proximity to the channel substrate would promote AKT1 phosphorylation by increasing locally the enzyme and substrate concentration.

While CIPK23, CIPK6, and CIPK16 interact with AKT1 (Xu et al., 2006; Lee et al., 2007), only CIPK15 is responsible for GORK activation (Forster et al., 2019). Our data suggest that the sequence variability of the residues making up the interaction surface of the ANK domain of plant VG channels may provide the basis for such specificity (Figs. 2 and 3; Supplemental Fig. S2). The regulation of AKT1, and also GORK, includes many different molecular partners, hormones, ions, and posttranslational modifications that ensure a finely tuned signal output in response to a particular input (Sánchez-Barrena et al., 2013; Xia et al., 2014; Edel and Kudla, 2016; Lefoulon et al., 2016; Behera et al., 2017; Chérel and Gaillard, 2019; Forster et al., 2019). Hence, the CIPK-ANK domain interaction may represent an additional component of a complex and multivalent set of interactions required to achieve specificity for channel activation (Fig. 6).

The joint analysis of our structural and biochemical data shows that the shallow nature of the concave side of the ANK domain of AKT1 provides an almost flat interface to interact with the catalytic domain of CIPK23 (Figs. 1 and 5A). This topology and the electrostatic nature of the interface (Fig. 2) suggest that the protein–protein interaction would not be restrictive (Krissinel and Henrick, 2007). However, our data show that the properties of the CIPK23 binding site at the ANK domain provide specificity for this kinase versus other CIPKs (Fig. 2). However, it should be noted that previous biochemical data showed that the specificity of the interaction between AKT1 and different CIPKs may not lay exclusively in the interaction between individual CIPKs and AKT1. Instead, the physical interaction between a particular CBL-CIPK complex and AKT1 could be the key to selectively activate the target channel (Xu et al., 2006; Lee et al., 2007). Phosphorylation of CBLs by their interacting CIPKs is a common event needed for the full competence of the CIPK-CBL module to regulate their target proteins (Du et al., 2011; Hashimoto et al., 2012), and could also help to stabilize the CIPK–CBL complex (Lin et al., 2009; Du et al., 2011). Accordingly, phosphorylation of CBL1 by CIPK23 is absolutely required for the CBL1-dependent enhancement of CIPK23 activity toward its substrate and the in vivo activation of the AKT1 channel in oocytes (Hashimoto et al., 2012). However, CBL9 can itself interact with AKT1 independently of CIPK23 (Grefen and Blatt, 2012), although the binding site has not been identified. Because CIPK23 uses different domains to interact with partners, i.e. the catalytic kinase domain to bind the ANK domain of AKT1 and the FISL/NAF domain to bind with CBL1/9, conceivably AKT1, CIPK23, and CBL1/9 could form a multiprotein complex via one-to-one interactions, thereby providing enhanced target specificity to the CIPK-CBL module. However, CBL4 and CBL10, which do not bind CIPK23, also interacted with AKT1 (Grefen and Blatt, 2012; Ren et al., 2013), and structural analyses of CIPK–CBL complexes have shown that the FISL/NAF domain of the bound CIPK occupies the hydrophobic cleft that enables the CBL to bind partners (Sánchez-Barrena et al., 2007; Akaboshi et al., 2008). This suggests that binding of CIPK23 and AKT1 to CBL1/9 could be mutually exclusive. Supporting this view, CBL10 competed with CIPK23 for binding to AKT1 and negatively modulated AKT1 activity (Ren et al., 2013). In conclusion, how the required specificity is achieved to

ensure non-promiscuous interactions between CIPK23 and the various Arabidopsis channels containing the ANK domain deserves further research. Altogether, the available data suggest that the CIPK23-ANK domain interaction, together with other sets of multiple and simultaneous low-affinity interactions (Fig. 6), could provide a regulation of K^+ homeostasis that would occur only when the interacting partners meet at the cell membrane in the vicinity of AKT1. This situation ensures an effective activation of the channel and warrants the versatility of the interacting partners to participate in different regulatory process.

Finally, the discovery of point mutations in the surface of the ANK domain of AKT1 that improve K^+ transport activity by strengthening the interaction with CIPK23 may represent a relevant biotechnological tool for the generation of plant crops with enhanced performance under K^+ nutrient limitation or other environmental stresses.

MATERIALS AND METHODS

Bio-Layer Interferometry

The interaction between the Arabidopsis (*Arabidopsis thaliana*) ANK domain of AKT1 and the catalytic domain of CIPK23 was measured by bio-layer interferometry using a single-channel BLItz system (ForteBio). His-tagged ANK domain and the mutated domains AKT1(−) (R528E K561E) and AKT1(+) (E624K E658K E659K) at 0.1 mg/mL were immobilized on Ni-chelated biosensor tips, and the purified domain of CIPK23 was added to the biosensor at three different concentrations to estimate the K_D value at room temperature. Each binding reaction was carried out in 50 mM of Tris HCl at pH 7.5 and 50 mM of NaCl, and consisted of a 30-s baseline, followed by a 300-s association phase and a 300-s dissociation phase. The software BLItz Pro (ForteBio) was used to determine rate constants for net association and dissociation, the equilibrium dissociation constant as the ratio of these values, and goodness of overall fit. Kinetic and affinity constants were calculated at CIPK23 concentrations of 16, 8, 4, and 2 μM; only those binding reactions producing goodness-of-fit values of X^2 and R^2 <4 and >0.99, respectively, were selected for the calculations.

SEC

The oligomeric state of the ANK domain of AKT1 was determined by SEC using a Bio-Silect SEC 250-5 Column (BioRad) equilibrated in 20 mM of Tris HCl at pH 8.0, 200 mM of NaCl, and 1 mM of DTT, and by comparing the elution time with that of the Gel Filtration Standard (BioRad).

Y2H Experiments

CIPK23 and *AKT1*cyt complementary DNAs (cDNAs) subcloned into the pGBT9.BS and the pGAD.GH vectors, respectively, have been described in Geiger et al. (2009). cDNAs of CIPK16 and CIPK24 in pGAD.GH (Kim et al., 2000) were isolated and transferred to pGBT9.BS. The AKT1cyt mutants AKT1(+) (E624K E658K E659K) and AKT1(−) (R528E K561E) were generated by PCR using pGAD.GH AKT1cyt as a template and the following primers: E624K (forward: gcacggcggctaagcaaggaaacttg, reverse: caagtttccttgcttagccg ccgtgc); E658K and E659K (forward: ccgctgtatgcaaaaagaacattgagatgg, reverse: caag tttccttgcttagccgccgtgc); R528E (forward: gctttgctgcaatagaagaagacgatttac, reverse: gtaaatcgtcttcttctattgcagcaaagc); and K561E (forward: gcatatagcagcatc agaaggaactcta aattgtg, reverse: cacaatttagagttccttctgatgctgctatatgc). Plasmids were cotransformed into *Saccharomyces cerevisiae* AH109 strain (*MATa trp1-901 leu2-3,112 ura3-52 his3-200 Gal4 gal80 URA3::MEL1UAS-MEL1TATALacZ LYS2::GAL1UAS-GAL1TATA-HIS3 GAL2UAS-GAL2TATA-ADE2*) after standard PEG/LiAc methods and colonies were selected on yeast synthetic dextrose (SD) minimal medium lacking Leu and Trp (SD−LT). To test interaction, transformant colonies of each combination of plasmids were grown in liquid SD−LT medium and 10-fold serial dilutions were spotted on SD plates lacking Leu, Trp, and His (SD−LTH). Yeast cells were incubated at 30°C for 4 d. Empty vectors were cotransformed as negative controls.

Functional Expression of AKT1 in Yeast

AKT1 was expressed in the *S. cerevisiae* strain 9.3 (*MAT*a, *ena1Δ::HIS3::ena4Δ*, *leu2*, *ura3*, *trp1*, *ade2*, *trk1Δ*, *trk2*::pCK64; Bañuelos et al., 1995). Wild-type AKT1 and mutant *AKT1ΔANK* cDNAs subcloned in the yeast expression vector pFL61 (Sentenac et al., 1992) were transformed in strain 9.3 using standard PEG/LiAc methods and colonies were selected on yeast synthetic minimal medium lacking uracil. Yeast cells were routinely grown in yeast peptone dextrose medium, 1% (w/v) yeast extract, 2% (w/v) peptone, and 2% (w/v) Glc or SD minimal medium supplemented with 50 mM of KCl. Growth tests in low-K^+ were performed in the alkali cation-free medium Arg Phosphate (AP; Rodríguez-Navarro and Ramos, 1984) solidified with 2% (w/v) noble agar (Difco) and supplemented with KCl at the concentrations indicated.

Crystallography

Details on gene cloning, protein expression, purification, and crystallization of the ANK domain of Arabidopsis AKT1 (residues from 516 to 706) can be found in Chaves-Sanjuán et al. (2014a). To summarize, an amplified gene product was cloned into pET-28a vector, overexpressed in *Escherichia coli* strain Rosetta 2(DE3) pLysS (Novagen), and purified by Ni^{2+}-NTA agarose bead affinity chromatography followed by SEC. Pure protein was concentrated to 14 mg mL^{-1} in a buffer containing 20 mM of HEPES at pH 7.0, 150 mM of NaCl, and 0.5 mM of TCEP and crystallized with sitting-drop vapor-diffusion techniques by equilibrating a mixture of 1 mL of protein solution and 1 mL of precipitant solution containing 25% (w/v) PEG4000, 0.1 M of Tris at pH 8.5, and 0.3 M of $MgCl_2$. Crystals grew in 3 d at room temperature. Crystals were cryoprotected with crystallization solution supplemented with 10% (v/v) glycerol.

A complete diffraction data set was collected at the European Synchrotron Radiation Facility (https://www.esrf.eu/) beamline ID14-1 (see details in Supplemental Table S1). Diffraction data were processed with the software XDS (Kabsch, 2010) and merged using the program Scala from the CCP4 package (Collaborative Computational Project, Number 4, 1994).

The strategy used to solve the structure of the ANK domain of AKT1 was molecular replacement with the program PHASER (McCoy et al., 2007) using the coordinates from a designed ankyrin domain (Protein Data Bank [PDB] code: 2XEH; Kramer et al., 2010). Several cycles of restrained refinement with the software tool PHENIX (Adams et al., 2010) and iterative model building with the software tool COOT (Emsley and Cowtan, 2004) were required to obtain the final models where the waters were also modeled. Data collection, data processing, and model refinement statistics are summarized in Supplemental Table S1. The stereochemistry of the models was verified with the program MolProbity (http://molprobity.biochem.duke.edu/) and figures of molecular models were produced using the software PyMOL (The PyMOL Molecular Graphics System, v1.6.0.0; Schrödinger).

Expression of Recombinant Proteins in *Xenopus laevis* Oocytes and Electrophysiological Procedures

The cDNAs of AKT1, AKT1(+), AKT1(−), and CIPK23HA, subcloned downstream of the T7 promoter in the vector pNB1u (MacAulay et al., 2001), were used to synthesize complementary RNA (cRNA) in vitro using the mMessage mMachine T7 Polymerase Kit (Ambion Europe). One microgram of cDNAs AKT1, AKT1(+), and AKT1(−) were linearized with the restriction enzyme *Not*I, whereas that of CIPK23HA was linearized with *Nde*I. The quality and purity of cRNAs were determined by absorbance at 260 and 280 nm (using a model no. ND-1000; NanoDrop Technologies). The integrity and size of the purified RNAs were checked by agarose gel electrophoresis (0.7% [w/v]) under denaturing conditions.

For electrical recordings of AKT1 activity, 50 nL of a cRNA mixture containing 14 ng of wild-type or mutant versions of AKT1 and 14 ng of CIPK23HA or 50 nL of distilled water (control) were injected in defolliculated oocytes of *X. laevis* using a Nanoliter 2010 Automatic Injector (World Precision Instruments). Injected oocytes were maintained at 18°C in ND96 solution (96 mM of NaCl, 2 mM of KCl, 1 mM of $CaCl_2$, 1 mM of $MgCl_2$, and 10 mM of HEPES/NaOH at pH 7.4). Two to 3 d after injection, the currents were measured at 20°C (room temperature) in two-electrode voltage-clamp experiments using the Geneclamp

500 Amplifier (Axon Instruments). Voltage control, data acquisition, and data analyses were carried out with the software Pulse/Pulsefit (HEKA). All electrodes were filled with 3 M of KCl solution. Two-electrode voltage-clamp recordings were obtained using a bath solution containing 2 mM of $MgCl_2$, 1 mM of $CaCl_2$, and 10 mM of Tris-HCl at pH 7.4 with the addition of 100 mM of KCl. Pulse protocols used a holding potential of −20 mV, followed by a test pulse to different voltage steps from −150 to +45 mV in 15-mV increments during 150 ms, separated by intervals of 2 s.

Protein–Protein Docking

Activated CIPK23 Kinase Model

Starting from the crystallographic structure of the CIPK23 kinase domain in the inactive conformation (PDB ID: 4CZT; Chaves-Sanjuan et al., 2014b), we employed the software MODELLER (Webb and Sali, 2016) to generate an active form of the enzyme based on the structure of the *Rattus norvegicus* 5′-AMP activated protein kinase α1 subunit (PDB ID: 4CFH). Only activation-related motifs were modeled (i.e. the Gly-rich loop, the hydrophobic spine, the activation loop, and the electrostatic lock). The resulting model was superimposed onto the structure of the Mn^{2+}-ATP-human PKA complex (PDB ID: 1ATP) to model the bound ATP and magnesium ions. The reconstructed activated Mg^{2+}-ATP-CIPK23 structure was refined using a standard protocol of energy minimization and MD simulation, employing the AMBER10 force field and optimized polyphosphate parameters. Briefly, the complex was immersed in a TIP3P water box (12 Å distance to the edge from any atom of the protein) and refined by means of 2,000 steps of steepest descent followed by 2,000 steps of conjugate gradient energy minimization. The energy-minimized structure was then heated to a temperature of 300 K while harmonically restraining the positions of the ATP molecule, the Mg^{2+} ions, and the Cα atoms of the protein. Thereafter, a production run spanning 40 ns allowed adaptation and relaxation of the amino acid side chains.

Protein–Protein Docking

An ensemble of activated CIPK23 conformations was obtained by clustering the structures generated during the MD simulation protocol. The structures were superimposed using their Cα atoms and their root-mean-square deviation was used as the similarity metric for an average linkage clustering algorithm (10 Å cutoff). The centroids of the top 10 most populated clusters were selected for protein–protein docking to account for kinase flexibility. The software Z-dock (Pierce et al., 2014) was employed to perform rigid docking of AKT1 on the ensemble of CIPK23 conformations, only considering the kinase amino acids described to be essential for binding (residues 97–132 and 267–300; Lee et al., 2007). A total of 2,000 solutions were extracted for each of the 10 kinase conformations. These solutions were reranked using the Z-rank (Pierce and Weng, 2007) scoring function (20,000 modeled complexes) to select a final list of 1,000 solutions that were subsequently clustered according to their root-mean-square deviation values. The top 10 clusters, according to the best energy value and top 10 most populated clusters, were selected for visual inspection. The final complex was selected using a combination of the score and degree of agreement with the catalytic function of the enzyme and experimental evidence available (essential regions for ANK domain binding).

The PDB formatted file of the calculated complex between the ANK domain of AKT1 and CIPK23 is provided in Supplemental Table S2.

Accession Numbers

The atomic coordinates and structure factors for the ankyrin domain of AKT1 (PDB: 5AAR) have been deposited in the Protein Data Bank (https://www.wwpdb.org/).

Supplemental Data

The following supplemental information is available.

Supplemental Figure S1. Representation of the crystal structures of the ANK domain of AKT1 and human Ankyin-R.

Supplemental Figure S2. Amino acid sequence alignment of the ANK domain of AKT1 and other plant protein homologs.

Supplemental Figure S3. Biophysical characterization of ANK domain of AKT1 using SEC and biolayer interferometry.

Supplemental Figure S4. Two views of a section of the predicted model for the complex between CIPK23 and the ANK domain of AKT1.

Supplemental Table S1. Crystallographic data collection and refinement statistics.

Supplemental Table S2. The atomic coordinates of the calculated complex between the ANK domain of AKT1 and CIPK23.

ACKNOWLEDGMENTS

A.A. thanks the European Synchrotron Radiation Facility and ALBA (beamlines ID23-2 and XALOC) for access to the synchrotron radiation source.

Received September 5, 2019; accepted January 23, 2020; published February 3, 2020.

LITERATURE CITED

Ache P, Becker D, Ivashikina N, Dietrich P, Roelfsema MR, Hedrich R (2000) GORK, a delayed outward rectifier expressed in guard cells of *Arabidopsis thaliana*, is a K^+-selective, K^+-sensing ion channel. FEBS Lett **486:** 93–98

Adams PD, Afonine PV, Bunkóczi G, Chen VB, Davis IW, Echols N, Headd JJ, Hung LW, Kapral GJ, Grosse-Kunstleve RW, et al (2010) PHENIX: A comprehensive Python-based system for macromolecular structure solution. Acta Crystallogr D Biol Crystallogr **66:** 213–221

Akaboshi M, Hashimoto H, Ishida H, Saijo S, Koizumi N, Sato M, Shimizu T (2008) The crystal structure of plant-specific calcium-binding protein AtCBL2 in complex with the regulatory domain of AtCIPK14. J Mol Biol **377:** 246–257

Albrecht V, Ritz O, Linder S, Harter K, Kudla J (2001) The NAF domain defines a novel protein–protein interaction module conserved in Ca^{2+}-regulated kinases. EMBO J **20:** 1051–1063

Alemán F, Caballero F, Ródenas R, Rivero RM, Martínez V, Rubio F (2014) The F130S point mutation in the Arabidopsis high-affinity K^+ transporter AtHAK5 increases K^+ over Na^+ and Cs^+ selectivity and confers Na^+ and Cs^+ tolerance to yeast under heterologous expression. Front Plant Sci **5:** 430

Alemán F, Nieves-Cordones M, Martínez V, Rubio F (2011) Root K^+ acquisition in plants: The *Arabidopsis thaliana* model. Plant Cell Physiol **52:** 1603–1612

Bañuelos MA, Klein RD, Alexander-Bowman SJ, Rodríguez-Navarro A (1995) A potassium transporter of the yeast *Schwanniomyces occidentalis* homologous to the Kup system of *Escherichia coli* has a high concentrative capacity. EMBO J **14:** 3021–3027

Batistic O, Waadt R, Steinhorst L, Held K, Kudla J (2010) CBL-mediated targeting of CIPKs facilitates the decoding of calcium signals emanating from distinct cellular stores. Plant J **61:** 211–222

Behera S, Long Y, Schmitz-Thom I, Wang XP, Zhang C, Li H, Steinhorst L, Manishankar P, Ren XL, Offenborn JN, et al (2017) Two spatially and temporally distinct Ca^{2+} signals convey *Arabidopsis thaliana* responses to K^+ deficiency. New Phytol **213:** 739–750

Chaves-Sanjuán A, Sánchez-Barrena MJ, González-Rubio JM, Albert A (2014a) Preliminary crystallographic analysis of the ankyrin-repeat domain of *Arabidopsis thaliana* AKT1: Identification of the domain boundaries for protein crystallization. Acta Crystallogr F Struct Biol Commun **70:** 509–512

Chaves-Sanjuan A, Sánchez-Barrena MJ, Gonzalez-Rubio JM, Moreno M, Ragel P, Jimenez M, Pardo JM, Martinez-Ripoll M, Quintero FJ, Albert A (2014b) Structural basis of the regulatory mechanism of the plant CIPK family of protein kinases controlling ion homeostasis and abiotic stress. Proc Natl Acad Sci USA **111:** E4532–E4541

Chérel I, Gaillard I (2019) The complex fine-tuning of K^+ fluxes in plants in relation to osmotic and ionic abiotic stresses. Int J Mol Sci **20:** 715

Chérel I, Lefoulon C, Boeglin M, Sentenac H (2014) Molecular mechanisms involved in plant adaptation to low K^+ availability. J Exp Bot **65:** 833–848

Daram P, Urbach S, Gaymard F, Sentenac H, Chérel I (1997) Tetramerization of the AKT1 plant potassium channel involves its C-terminal cytoplasmic domain. EMBO J **16:** 3455–3463

Du W, Lin H, Chen S, Wu Y, Zhang J, Fuglsang AT, Palmgren MG, Wu W, Guo Y (2011) Phosphorylation of SOS3-like calcium-binding proteins by their interacting SOS2-like protein kinases is a common regulatory mechanism in Arabidopsis. Plant Physiol **156:** 2235–2243

Edel KH, Kudla J (2016) Integration of calcium and ABA signaling. Curr Opin Plant Biol **33:** 83–91

Emsley P, Cowtan K (2004) COOT: Model-building tools for molecular graphics. Acta Crystallogr D Biol Crystallogr **60:** 2126–2132

Forster S, Schmidt LK, Kopic E, Anschutz U, Huang S, Schlucking K, Koster P, Waadt R, Larrieu A, Batistic O, et al (2019) Wounding-induced stomatal closure requires jasmonate-mediated activation of GORK K^+ channels by a Ca^{2+} sensor-kinase CBL1-CIPK5 complex. Dev Cell **48:** 87–99 e86

Gao Y, Cao E, Julius D, Cheng Y (2016) TRPV1 structures in nanodiscs reveal mechanisms of ligand and lipid action. Nature **534:** 347–351

Geiger D, Becker D, Vosloh D, Gambale F, Palme K, Rehers M, Anschuetz U, Dreyer I, Kudla J, Hedrich R (2009) Heteromeric AtKC1●AKT1 channels in Arabidopsis roots facilitate growth under K^+-limiting conditions. J Biol Chem **284:** 21288–21295

Gong D, Guo Y, Schumaker KS, Zhu JK (2004) The SOS3 family of calcium sensors and SOS2 family of protein kinases in Arabidopsis. Plant Physiol **134:** 919–926

Grefen C, Blatt MR (2012) Do calcineurin B-like proteins interact independently of the serine threonine kinase CIPK23 with the K^+ channel AKT1? Lessons learned from a ménage à trois. Plant Physiol **159:** 915–919

Guo Y, Halfter U, Ishitani M, Zhu JK (2001) Molecular characterization of functional domains in the protein kinase SOS2 that is required for plant salt tolerance. Plant Cell **13:** 1383–1400

Hashimoto K, Eckert C, Anschütz U, Scholz M, Held K, Waadt R, Reyer A, Hippler M, Becker D, Kudla J (2012) Phosphorylation of calcineurin B-like (CBL) calcium sensor proteins by their CBL-interacting protein kinases (CIPKs) is required for full activity of CBL-CIPK complexes toward their target proteins. J Biol Chem **287:** 7956–7968

Hedrich R, Geiger D (2017) Biology of SLAC1-type anion channels—from nutrient uptake to stomatal closure. New Phytol **216:** 46–61

Hirsch RE, Lewis BD, Spalding EP, Sussman MR (1998) A role for the AKT1 potassium channel in plant nutrition. Science **280:** 918–921

Hosy E, Vavasseur A, Mouline K, Dreyer I, Gaymard F, Porée F, Boucherez J, Lebaudy A, Bouchez D, Very AA, et al (2003) The Arabidopsis outward K^+ channel GORK is involved in regulation of stomatal movements and plant transpiration. Proc Natl Acad Sci USA **100:** 5549–5554

Hubbard SJ, Thornton JM (1993) NACCESS Computer Program. Department of Biochemistry and Molecular Biology, University College London, London

Jegla T, Busey G, Assmann SM (2018) Evolution and structural characteristics of plant voltage-gated K^+ channels. Plant Cell **30:** 2898–2909

Kabsch W (2010) XDS. Acta Crystallogr D Biol Crystallogr **66:** 125–132

Kelley LA, Mezulis S, Yates CM, Wass MN, Sternberg MJ (2015) The Phyre2 web portal for protein modeling, prediction and analysis. Nat Protoc **10:** 845–858

Keskin O, Gursoy A, Ma B, Nussinov R (2008) Principles of protein–protein interactions: What are the preferred ways for proteins to interact? Chem Rev **108:** 1225–1244

Kim KN, Cheong YH, Gupta R, Luan S (2000) Interaction specificity of Arabidopsis calcineurin B-like calcium sensors and their target kinases. Plant Physiol **124:** 1844–1853

Kohl A, Binz HK, Forrer P, Stumpp MT, Plückthun A, Grütter MG (2003) Designed to be stable: Crystal structure of a consensus ankyrin repeat protein. Proc Natl Acad Sci USA **100:** 1700–1705

Kramer MA, Wetzel SK, Plückthun A, Mittl PR, Grütter MG (2010) Structural determinants for improved stability of designed ankyrin repeat proteins with a redesigned C-capping module. J Mol Biol **404:** 381–391

Krissinel E, Henrick K (2007) Inference of macromolecular assemblies from crystalline state. J Mol Biol **372:** 774–797

Lagarde D, Basset M, Lepetit M, Conejero G, Gaymard F, Astruc S, Grignon C (1996) Tissue-specific expression of Arabidopsis AKT1 gene is consistent with a role in K^+ nutrition. Plant J **9:** 195–203

Lan WZ, Lee SC, Che YF, Jiang YQ, Luan S (2011) Mechanistic analysis of AKT1 regulation by the CBL-CIPK-PP2CA interactions. Mol Plant **4:** 527–536

Lee CH, MacKinnon R (2017) Structures of the human HCN1 hyperpolarization-activated channel. Cell **168:** 111–120 e111

Lee SC, Lan W, Buchanan BB, Luan S (2009) A protein kinase–phosphatase pair interacts with an ion channel to regulate ABA signaling in plant guard cells. Proc Natl Acad Sci USA **106:** 21419–21424

Lee SC, Lan WZ, Kim BG, Li L, Cheong YH, Pandey GK, Lu G, Buchanan BB, Luan S (2007) A protein phosphorylation/dephosphorylation network regulates a plant potassium channel. Proc Natl Acad Sci USA **104:** 15959–15964

Lefoulon C, Boeglin M, Moreau B, Véry AA, Szponarski W, Dauzat M, Michard E, Gaillard I, Chérel I (2016) The Arabidopsis AtPP2CA protein phosphatase inhibits the GORK K^+ efflux channel and exerts a dominant suppressive effect on phosphomimetic-activating mutations. J Biol Chem **291:** 6521–6533

Leigh RA, Wyn Jones RG (1984) A hypothesis relating critical potassium concentrations for growth to the distribution and functions of this ion in the plant cell. New Phytol **97:** 1–13

Lin H, Yang Y, Quan R, Mendoza I, Wu Y, Du W, Zhao S, Schumaker KS, Pardo JM, Guo Y (2009) Phosphorylation of SOS3-LIKE CALCIUM BINDING PROTEIN8 by SOS2 protein kinase stabilizes their protein complex and regulates salt tolerance in Arabidopsis. Plant Cell **21:** 1607–1619

Luan S (2009) The CBL–CIPK network in plant calcium signaling. Trends Plant Sci **14:** 37–42

MacAulay N, Gether U, Klarke DA, Zeuthen T (2001) Water transport by the human Na^+-coupled glutamate cotransporter expressed in Xenopus oocytes. J Physiol **530:** 367–378

Maierhofer T, Diekmann M, Offenborn JN, Lind C, Bauer H, Hashimoto K, S Al-Rasheid KA, Luan S, Kudla J, Geiger D, et al (2014) Site- and kinase-specific phosphorylation-mediated activation of SLAC1, a guard cell anion channel stimulated by abscisic acid. Sci Signal **7:** ra86

McCoy AJ, Grosse-Kunstleve RW, Adams PD, Winn MD, Storoni LC, Read RJ (2007) Phaser crystallographic software. J Appl Cryst **40:** 658–674

Michaely P, Tomchick DR, Machius M, Anderson RG (2002) Crystal structure of a 12 ANK repeat stack from human ankyrinR. EMBO J **21:** 6387–6396

Mosavi LK, Minor DL Jr., Peng ZY (2002) Consensus-derived structural determinants of the ankyrin repeat motif. Proc Natl Acad Sci USA **99:** 16029–16034

Nooren IM, Thornton JM (2003) Diversity of protein–protein interactions. EMBO J **22:** 3486–3492

Pardo JM (2010) Biotechnology of water and salinity stress tolerance. Curr Opin Biotechnol **21:** 185–196

Paulsen CE, Armache JP, Gao Y, Cheng Y, Julius D (2015) Structure of the TRPA1 ion channel suggests regulatory mechanisms. Nature **520:** 511–517

Perkins JR, Diboun I, Dessailly BH, Lees JG, Orengo C (2010) Transient protein–protein interactions: Structural, functional, and network properties. Structure **18:** 1233–1243

Pierce B, Weng Z (2007) ZRANK: Reranking protein docking predictions with an optimized energy function. Proteins **67:** 1078–1086

Pierce BG, Wiehe K, Hwang H, Kim BH, Vreven T, Weng Z (2014) ZDOCK server: Interactive docking prediction of protein–protein complexes and symmetric multimers. Bioinformatics **30:** 1771–1773

Pilot G, Pratelli R, Gaymard F, Meyer Y, Sentenac H (2003) Five-group distribution of the *Shaker*-like K^+ channel family in higher plants. J Mol Evol **56:** 418–434

Ragel P, Raddatz N, Leidi EO, Quintero FJ, Pardo JM (2019) Regulation of K^+ nutrition in plants. Front Plant Sci **10:** 281

Ragel P, Rodenas R, Garcia-Martin E, Andrés Z, Villalta I, Nieves-Cordones M, Rivero RM, Martínez V, Pardo JM, Quintero FJ, et al (2015) The CBL-interacting protein kinase CIPK23 regulates HAK5-mediated high-affinity K^+ uptake in Arabidopsis roots. Plant Physiol **169:** 2863–2873

Ren XL, Qi GN, Feng HQ, Zhao S, Zhao SS, Wang Y, Wu WH (2013) Calcineurin B-like protein CBL10 directly interacts with AKT1 and modulates K^+ homeostasis in Arabidopsis. Plant J **74:** 258–266

Rodríguez-Navarro A (2000) Potassium transport in fungi and plants. Biochim Biophys Acta **1469:** 1–30

Rodríguez-Navarro A, Ramos J (1984) Dual system for potassium transport in *Saccharomyces cerevisiae*. J Bacteriol **159:** 940–945

Sánchez-Barrena MJ, Fujii H, Angulo I, Martínez-Ripoll M, Zhu JK, Albert A (2007) The structure of the C-terminal domain of the protein kinase AtSOS2 bound to the calcium sensor AtSOS3. Mol Cell **26:** 427–435

Sánchez-Barrena MJ, Martínez-Ripoll M, Albert A (2013) Structural biology of a major signaling network that regulates plant abiotic stress: The CBL-CIPK mediated pathway. Int J Mol Sci **14:** 5734–5749

Sedgwick SG, Smerdon SJ (1999) The ankyrin repeat: A diversity of interactions on a common structural framework. Trends Biochem Sci **24:** 311–316

Sentenac H, Bonneaud N, Minet M, Lacroute F, Salmon JM, Gaymard F, Grignon C (1992) Cloning and expression in yeast of a plant potassium ion transport system. Science **256:** 663–665

Shi J, Kim KN, Ritz O, Albrecht V, Gupta R, Harter K, Luan S, Kudla J (1999) Novel protein kinases associated with calcineurin B-like calcium sensors in Arabidopsis. Plant Cell **11:** 2393–2405

Sultana A, Lee JE (2015) Measuring protein–protein and protein–nucleic acid interactions by biolayer interferometry. Curr Protoc Protein Sci **79:** 19–25

Tamaskovic R, Simon M, Stefan N, Schwill M, Plückthun A (2012) Designed ankyrin repeat proteins (DARPins) from research to therapy. Methods Enzymol **503:** 101–134

Tang Q, Guo W, Zheng L, Wu JX, Liu M, Zhou X, Zhang X, Chen L (2018) Structure of the receptor-activated human TRPC6 and TRPC3 ion channels. Cell Res **28:** 746–755

Wang Y, He L, Li HD, Xu J, Wu WH (2010) Potassium channel alpha-subunit AtKC1 negatively regulates AKT1-mediated K^+ uptake in Arabidopsis roots under low-K^+ stress. Cell Res **20:** 826–837

Webb B, Sali A (2016) Comparative protein structure modeling using MODELLER. Curr Protoc Bioinformatics **54:** 5.6.1-5.6.37

Whicher JR, MacKinnon R (2016) Structure of the voltage-gated K^+ channel Eag1 reveals an alternative voltage sensing mechanism. Science **353:** 664–669

Xia J, Kong D, Xue S, Tian W, Li N, Bao F, Hu Y, Du J, Wang Y, Pan X, et al (2014) Nitric oxide negatively regulates AKT1-mediated potassium uptake through modulating vitamin B6 homeostasis in Arabidopsis. Proc Natl Acad Sci USA **111:** 16196–16201

Xu J, Li HD, Chen LQ, Wang Y, Liu LL, He L, Wu WH (2006) A protein kinase, interacting with two calcineurin B-like proteins, regulates K^+ transporter AKT1 in Arabidopsis. Cell **125:** 1347–1360